A triplet of differently shaped spin-zero states in the atomic nucleus ^{186}Pb

A. N. Andreyev*, M. Huyse*, P. Van Duppen*, L. Weissman*, D. Ackermann†, J. Gerl†, F. P. Heßberger†, S. Hofmann†, A. Kleinböhl†, G. Münzenberg†, S. Reshitko†, C. Schlegel†, H. Schaffner†, P. Cagarda‡, M. Matos‡, S. Saro‡, A. Keenan§, C. Moore§, C. D. O'Leary§, R. D. Page§, M. Taylor§, H. Kettunen‖, M. Leino‖, A. Lavrentiev¶, R. Wyss# & K. Heyde☆

** Instituut voor Kern- en Stralingsfysica, University of Leuven, Celestijnenlaan 200 D, B-3001 Leuven, Belgium*
† Gesellschaft fur Schwerionenforschung Darmstadt, Postfach 110541, D-6100 Darmstadt, Germany
‡ Department of Nuclear Physics, Comenius University, Bratislava, Slovakia
§ Department of Physics, Oliver Lodge Laboratory, University of Liverpool, Liverpool L69 7ZE, UK
‖ Department of Physics, University of Jyväskylä, FIN-40351 Jyväskylä, Finland
¶ Flerov Laboratory of Nuclear Reactions, Joint Institute for Nuclear Research, 141980 Dubna, Russia
 # Department of Physics, Royal Institute of Technology, 104 05 Stockholm, Sweden, and Department of Technology, Kalmar University, Box 905, 391 29 Kalmar, Sweden
☆ Vakgroep Subatomaire en Stralingsfysica, Institute for Theoretical Physics, B-9000 Gent, Belgium

Understanding the fundamental excitations of many-fermion systems is of significant current interest. In atomic nuclei with even numbers of neutrons and protons, the low-lying excitation spectrum is generally formed by nucleon pair breaking and nuclear vibrations or rotations. However, for certain numbers of protons and neutrons, a subtle rearrangement of only a few nucleons among the orbitals at the Fermi surface can result in a different elementary mode: a macroscopic shape change[1–3]. The first experimental evidence for this phenomenon came from the observation of shape coexistence in ^{16}O (ref. 4). Other unexpected examples came with the discovery of fission isomers[5] and superdeformed nuclei[6]. Here we find experimentally that the lowest three states in the energy spectrum of the neutron deficient nucleus ^{186}Pb are spherical, oblate and prolate. The states are populated by the α-decay of a parent nucleus; to identify them, we combine knowledge of the particular features of this decay[7] with sensitive measurement techniques (a highly efficient velocity filter[8] with strong background reduction, and an extremely selective recoil-α-electron coincidence tagging method[8–10]). The existence of this apparently unique shape triplet is permitted only by the specific conditions that are met around this particular nucleus.

The study of a system of A nucleons bound together by nucleon–nucleon interaction in an atomic nucleus poses a complex problem. The rich spectrum of elementary modes of collective motion, such as rotations and vibrations, is very difficult to derive from the action of the nucleon–nucleon force. Instead, these phenomena can be described as emerging from the interplay of the constituent particles and the use of effective forces. In this context, the atomic nucleus which, at the lower energy scale is now understood as behaving very much like a superfluid system, can be compared to complex mesoscopic systems of the type that appears in atomic cluster structures and low-dimensional quantum systems (integer and fractional quantum Hall effect). This is due to the number of nucleons (of the order of 100 in an average nucleus), which is too large for a full microscopic study but also too small for statistical treatments. The variety of shapes in atomic nuclei and the effect of individual nucleons continue to be a topic of current research (see ref. 11 for a review).

The lowest excitation mode encountered in atomic nuclei is, in general, associated with rotations. In the mass $A = 170$ region, the observed moment of inertia (J) of a deformed nucleus lies between the values corresponding to a rigid object and a fluid, and leads to a rotational energy constant of the order of $\hbar^2/2J \approx 15$ keV. But because some nucleon numbers are found to be 'magic' (N or $Z = 8$, 20, 28, 50, 82, 126 (or $Z \approx 114$)), nuclei with a closed shell are predominantly spherical and as such do not exhibit rotational excitations at low energy. Due to the stiffness of the closed configuration, vibrations will also be hindered and the first excitations will be due to breaking a pair of nucleons from the open shell. The resulting spectrum is a typical one-broken-pair multiplet and leads in the even–even Pb ($Z = 82$) nuclei to a first excited state around 1 MeV with spin and parity 2^+, except for doubly magic ^{208}Pb which has a 3^- level at 2.6 MeV as its first excited state.

A new phenomenon occurs in the neutron-deficient Pb nuclei, where the number of valence neutrons becomes maximal as the neutron number lies in the middle of two numbers characteristic of closed shells ($N = 82$ and $N = 126$)[1,2]. Within a shell-model approach[2], a proton pair excitation across the $Z = 82$ shell leads to the creation of two valence proton particles (2p) above, and two valence proton holes (2h) below, the $Z = 82$ closed shell, that are coupled to spin and parity 0^+. The energy cost is about twice the energy of the $Z = 82$ shell gap ($\approx 2 \times 3.9$ MeV $= 7.8$ MeV) but the creation of one particle and one hole pair yields a gain in pairing correlation energy of 2.6 MeV which can be derived from the experimental one- and two-proton separation energies[2]. Furthermore, the proton shell is now broken up and the attractive proton–neutron interaction will lower the energy for these 2p–2h states, so that from ^{194}Pb onwards this 0^+ state lies below the first excited 2^+ state[3]. Within a deformed mean-field approach this is equivalent to a macroscopic phase change from a spherical to an oblate shape[12]. The band structure built on top of it has been observed only for a limited number of neutron-deficient Pb nuclei, the lightest being

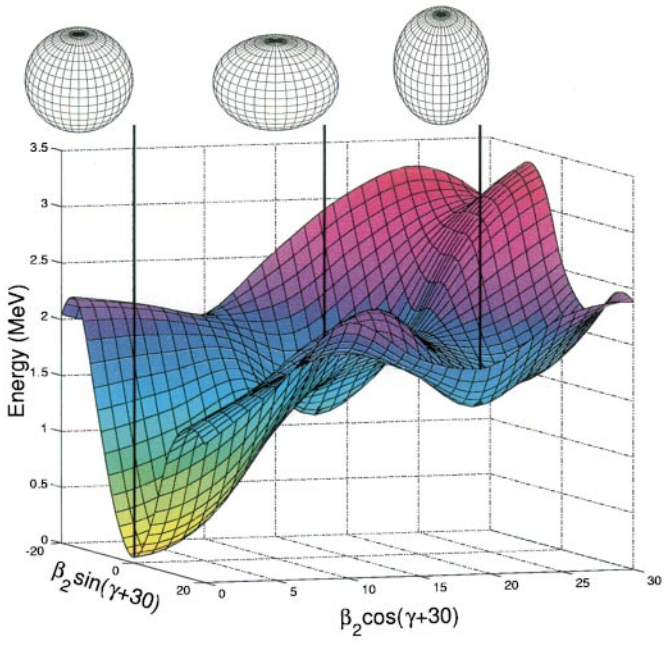

Figure 1 Calculated potential energy surface of ^{186}Pb. Spherical, oblate and prolate minima are indicated by thick vertical black lines. Calculations are performed on the cartesian mesh. The β_2 parameter expresses the elongation of the nucleus along the symmetry axis, while the γ parameter relates to the degree of triaxiality in the deformation (that is, the relative lengths of the three principal axes of the spheroidal nucleus). The γ parameter is defined such that $\gamma = 0$ corresponds to a prolate (cigar-like) shape and $\gamma = 60$ to an oblate (disk-like) shape.

^{190}Pb (ref. 13). This schematic picture can also be extended to multi-particle and multi-hole excitations, each of them possibly leading to a different shape.

The energy of the different shape configurations can be calculated using a nucleon potential, such as the Woods–Saxon[14] potential, in which the energy of a single-particle orbital depends on the deformation. These potential-energy-surface calculations have become more and more sophisticated with time, resulting in accurate descriptions of the nuclear shapes and the configurations involved[14–16]. Figure 1 gives the result of such a calculation for ^{186}Pb and shows, next to the spherical minimum corresponding to the ground state, an oblate and a prolate minimum at an excitation energy of around 1 MeV. In the particle–hole picture, the former corresponds to a 2p–2h configuration, while the latter corresponds to a 4p–4h configuration as discussed in ref. 15. It is of prime importance to identify and to characterize the three 0^+ states associated with the three different shapes.

Alpha decay forms an ideal tool to populate the 0^+ bandheads and probe selectively the underlying structure[7]; this has led to the identification of the oblate 2p–2h bandheads down to $^{188}_{82}Pb_{106}$, where a bandhead was observed at $E^* = 591$ keV (ref. 9, 17, 18) above the spherical ground state and was recently confirmed by in-beam electron spectroscopy[19]. In-beam studies showed rotational bands in ^{184,186,188}Pb associated only with a prolate-deformed shape[20–22]. Conflicting results on the prolate 4p–4h 0^+ bandhead in ^{188}Pb have been reported, giving two different values of 767(12) keV (ref. 9) (α-decay study) and 725(4) keV (ref. 19) (conversion-electron spectroscopy). (Here 767(12) keV, for example, indicates 767 ± 12 keV.) The exotic nucleus ^{186}Pb, far away from the stability line but with a closed proton shell and with the neutrons exactly at mid-shell between $N = 82$ and $N = 126$, represents a unique opportunity to study the competition between shape excitations, collective motion and intrinsic excitations. This maximum in proton–neutron correlations will enable the study of shape coexistence at the lowest possible excitation energy. The relative positions of the three different shapes, the height of the barrier between them, and consequently the purity of the configurations, are further aspects that can be addressed in this nucleus.

To study in detail ^{186}Pb through the α-decay of ^{190}Po is a challenging task. The ^{190}Po nuclei are produced via the 4n-evaporation channel for the fusion reaction of 200-pnA ($= 1.2 \times 10^{12}$ particles per s) 255-MeV ^{52}Cr ions with a 290 μg cm^{-2} $^{142}NdF_3$ target. The cross-section is only about 300 nbarn ($= 3 \times 10^{-31}$ cm^2) which corresponds to about 300 ^{190}Po atoms being produced per hour but with a background of fission and transfer reactions about a million times higher. The Separator for Heavy Ion Production (SHIP) velocity filter[8], developed for the studies of superheavy elements, is able to separate the nuclei of interest from unwanted background and to implant them into an efficient detection system[8,10] (see Fig. 2 and its legend for further details). The experimental set-up has been optimized to observe fine structure in the α-decay that leads, as studied for the heavier even–even Pb nuclei[7], to the identification of low-lying 0^+ bandheads, which will decay predominantly by E0 conversion electron transitions to the ground state.

The data in Fig. 3 form the main evidence for the observation of three different shapes in ^{186}Pb. Out of the 27,080 counts recorded in Fig. 3a, only 274 show (see Fig. 3b) coincidence with electrons, as observed from the two peak structures at 7,012(20) and 6,896(20) keV. As seen in Fig. 3c, these peaks are almost completely decayed within 12 ms. The half-life of the 7,012-keV line is 2.6(0.3) ms, while for the 6,896-keV line an upper limit of 5 ms for the short-lived component is obtained. Only two isotopes shown in Fig. 3a have such a short half-life: ^{190}Po, 2.45(5) ms (this work); and ^{189m}Bi, 5.0(1) ms (ref. 10). All the other isotopes have considerably longer half-lives (see Fig. 3a). The behaviour of the ^{189m}Bi isotope was studied at different beam energies, and it can be concluded that α–e coincidences from fine structure in the α-decay

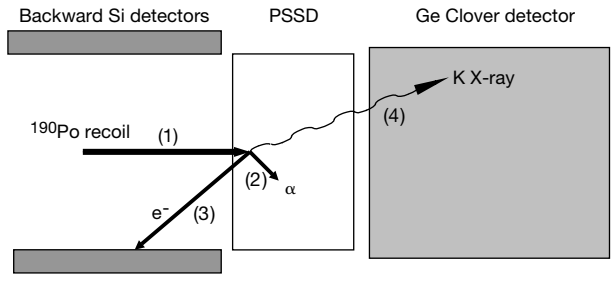

Figure 2 A view of the detector system (not to scale). Owing to the segmentation of the position sensitive silicon detector (PSSD) and the low implantation rate, it is possible to correlate the time and position of the implanted recoil products and their subsequent α-decays (recoil-α correlations). Six Si detectors (the Si box) are mounted in front of the PSSD ('backward') to detect conversion electrons in prompt coincidence with the α-decay (recoil-α-e$^-$ correlations). A 4-fold segmented Ge Clover detector records prompt α-X and α-γ coincidences. A schematic picture of a recoil (1) –α (2) –e$^-$ (3) –X (4) event is given. The identification of the different α lines is based on the half-life, the count rate as a function of the bombarding energy (5 different beam energies), coincidences with electrons, characteristic K-X rays and γ lines, correlations with known α-decay of daughters in the decay chain, and sum-energy relations.

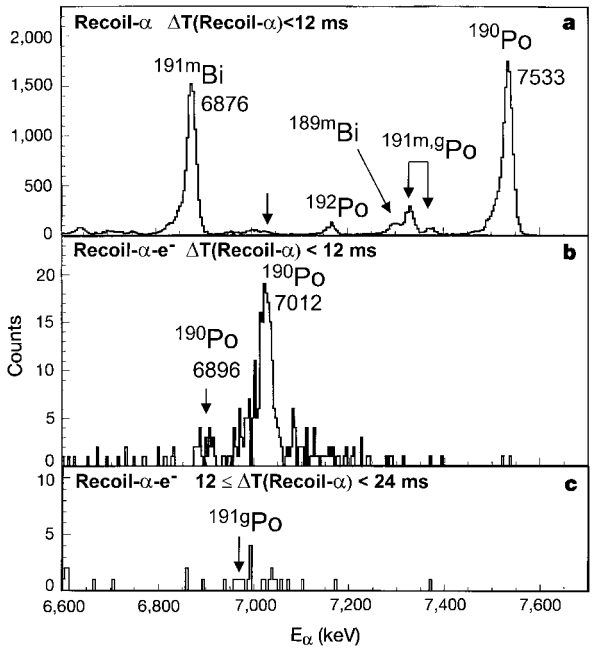

Figure 3 Three α spectra with different gating conditions. **a**, Part of the α spectrum recorded in the PSSD within 12 ms after the recoil implantation. Some peaks are labelled with the α-decay energy and isotope they relate to, with the label g for the ground state and m for an isomeric state for the same isotope. The strongest α line is the ground-state to ground-state α transition of ^{190}Po at 7,533(10) keV decaying with a half-life of 2.45(5) ms, an improved value compared to literature[18,23]. The other α lines are from isotopes produced in other open evaporation channels (xn, pxn). They have been identified on the basis of their energy, half-life and yield as a function of the beam energy (excitation function). The main isotopes are: ^{191m}Bi, $T_{1/2} = 115(10)$ ms (ref. 24); ^{192}Po, $T_{1/2} = 33.4(14)$ ms (ref. 17); ^{189m}Bi, $T_{1/2} = 5.0(1)$ ms (ref. 10); ^{191m}Po, $T_{1/2} = 98(8)$ ms (ref. 25); ^{191g}Po, $T_{1/2} = 22(1)$ ms (ref. 25). **b**, The same as **a**, but in a prompt coincidence with conversion electrons, registered in the backward detectors. The random background probability is 7×10^{-5}. **c**, The same prompt electron condition as in **b**, but now with α events that are registered between 12 and 24 ms after implantation.

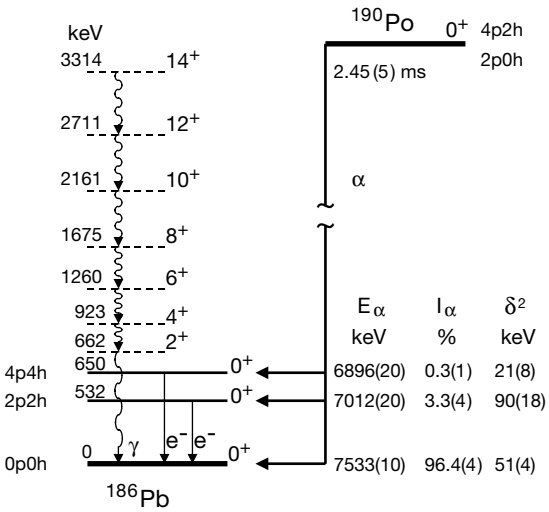

Figure 4 The decay pattern of ^{190}Po and the level scheme of ^{186}Pb. Indicated are α-decay energies E_α, intensities I_α, reduced α-widths δ^2, and configuration assignments. As discussed in ref. 7, the reduced α widths δ^2 for the even-mass Po, Pb, Hg and Pt nuclei around $N = 104$ lie around 70 keV. Lower (higher) values indicate retarded (enhanced) transitions. The known prolate rotational band ($I^\pi = 2^+ \rightarrow 14^+$) is shown by dashed lines[21,22].

of ^{189m}Bi (ref. 10) do not contribute to the spectrum in Fig. 3b. The only coincidences that the two lines observed in Fig. 3b show with Ge detectors are in the region of low-energy X-rays below 100 keV, and the 7,012-keV α line is clearly coincident with the characteristic K X-rays of Pb. Furthermore, both lines correlate with the α line of ^{186}Pb, the daughter of ^{190}Po. Therefore the 7,012 and 6,896 keV α lines are attributed to the decay of ^{190}Po. The counts in the region between 6,800 and 7,000 keV in Fig. 3c) can be explained by coincidences with conversion electrons from electromagnetic transitions, recently reported in the decay of ^{191m,g}Po (refs 24, 25). Their decay is partly responsible for the left shoulder of the 7,012-keV peak observed in Fig. 3b, and for the weak long-lived component under the 6,896-keV line. The extra counts above the 7,012-keV peak (Fig. 3b) are due to an electron sharing its energy between the position-sensitive silicon detector and the Si box, thus partially adding to the α line. By comparing the coincidences of the 7,012 and 6,896 keV α lines with electrons, X- and γ-rays, the only valid conclusion is to assign the two lines as fine structure lines due to α-decay of ^{190}Po feeding excited levels in ^{186}Pb, subsequently decaying by E0 conversion electron emission to the ground state (Fig. 4).

From the reduced α-decay widths δ^2 of $\Delta l = 0$ transitions, which correspond to the transition rate after correcting for the energy dependence from the tunnelling through the Coulomb barrier, it is possible to obtain information on the internal structure of the configurations involved in the connected states[7,26,27]. This method has been used to show that the ground state of ^{186}Pb is spherical, as are all heavier even–even Pb nuclei[26,28]. The ground states of even–even Po nuclei with $A > 196$ exhibit a spherical 2p proton configuration. However, owing to the rapid lowering in energy of deformed 4p–2h proton configurations, the ground states of the lighter even–even Po nuclei, from ^{196}Po onwards[27], develop a mixed character of 2p and 4p–2h configuration (with ~70% of the latter in the ground state of ^{192}Po; refs 9, 17). The reduced widths in the α-decay of ^{190}Po (see Fig. 4) and ^{192}Po corroborate this superposition, and unambiguously show that the decay to the 0p–0h spherical ground state in ^{186}Pb is much slower than the decay to the first excited 0^+ state. This indicates that the ground state of ^{190}Po is mainly the deformed 4p–2h configuration, and that the first excited 0^+ state in ^{186}Pb has a multiparticle–multihole character. Based on the energy systematic of the oblate bandheads in the heavier Pb isotopes, the extrapolation of the 0^+ bandhead energy starting from the higher-spin members of the prolate band in ^{186}Pb (see Fig. 4), and the reduced α-widths, we identify the 0^+ state (with an excitation energy of 532 keV) as the oblate state, and the 0^+ state (with an excitation energy of 650 keV) as the prolate state. Both of these levels are below the first excited 2^+ state, at 662 keV.

This observation allows to consider the atomic nucleus ^{186}Pb as a 'laboratory' in which to observe the effect of a change of a small number of particles on the macroscopic shape. The energy gap at the $Z = 82$ closed shell (~3.9 MeV) forces the protons to adopt a spherical shape, while the large space available for the valence neutrons (with N values between 82 and 126) favours a deformed configuration. Combined with the strength of the proton–neutron quadrupole force and the pairing[2], a subtle balance originates where the promotion of specific proton pairs to the next shell leads to either a prolate or to an oblate state. Proceeding to lighter masses (towards Sn and Ni), the steady increase in the shell gap energy, combined with a decreasing open space for the valence particles, lead to an increase in excitation energy of the deformed states. For the heavier elements (beyond Pb), the shell gap becomes too small and the proton–neutron correlation energy causes the ground state to become deformed. Only in the neutron-deficient Pb region are the exact conditions met to study, near the ground state (in a zone of low-level density), the microscopic origin of the spherical-symmetry breaking which leads to spheroidal deformation. Other systems having the character of Fermi liquids, such as atomic and molecular clusters, also exhibit shell structure and deformation. However, the large moments of inertia make rotation the easiest way by far to excite the system ($\hbar^2/2J \approx 10^{-4}$ eV) thereby complicating the observation of shape changes.

The study presented here has used α-decay as a spectroscopic tool to elucidate this triple shape coexistence. Nuclear physics has developed a whole arsenal of spectroscopic methods to identify and characterize the collective behaviour of quantum liquids. The observation of band structures build upon different shapes and their interaction will further probe the purity of the states and their evolution when excited. □

Received 20 December 1999; accepted 3 April 2000.

1. Heyde, K. *et al.* Coexistence in odd-mass nuclei. *Phys. Rep.* **102,** 291–393 (1983).
2. Wood, J. L. *et al.* Coexistence in even-mass nuclei. *Phys. Rep.* **215**, 101–201 (1992).
3. Van Duppen, P. *et al.* Observation of low-lying $J^\pi = 0^+$ states in the single-closed shell nuclei $^{192\text{-}198}$Pb. *Phys. Rev. Lett.* **52,** 1974–1977 (1984).
4. Morinaga, H. Interpretation of some excited states of 4n self-conjugate nuclei. *Phys. Rev.* **101,** 254–258 (1956).
5. Bjørnholm, S. & Lynn, J. E. The double-humped fission barrier. *Rev. Mod. Phys.* **52,** 725–931 (1980).
6. Nolan, P. & Twin, P. Superdeformed states at high angular momentum. *Annu. Rev. Nucl. Part. Sci.* **38,** 533–562 (1988).
7. Van Duppen, P. & Huyse, M. Shape coexistence around the Z = 82 closed shell probed by α decay. *Hyperfine Interact.* (in the press).
8. Hofmann, S. New elements—approaching Z = 114. *Rep. Prog. Phys.* **69,** 827–888 (1998).
9. Allatt, R. G. *et al.* Fine structure in ^{192}Po α-decay and shape coexistence in ^{188}Pb. *Phys. Lett. B* **437,** 29–34 (1998).
10. Andreyev, A. N. *et al.* Alpha decay of the new isotopes ^{188,189}Po. *Eur. Phys. J. A* **6**, 381–385 (1999).
11. Walker, P. & Dracoulis, G. D. Energy traps in atomic nuclei. *Nature* **399,** 35–40 (1999).
12. Heyde, K. *et al.* Equivalence of the spherical and deformed shell-model approach to intruder states. *Phys. Lett. B* **218,** 287–290 (1989).
13. Dracoulis, G. D. *et al.* Interference between spherical and deformed states in ^{190}Pb. *Phys. Lett. B* **432,** 37–44 (1998).
14. Cwiok, S. *et al.* Axially deformed Woods-Saxon potential. *Comput. Phys. Commun.* **46,** 379–399 (1987).
15. Nazarewicz, W. Variety of shapes in the mercury and lead isotopes. *Phys. Lett. B* **305,** 195–201 (1993).
16. Tajima, N. *et al.* Diabatic effects in ^{186}Pb: a generator-coordinate analysis. *Nucl. Phys. A* **551,** 409–433 (1993).
17. Bijnens, N. *et al.* Fine structure in the α decay of ^{192}Po. *Z. Phys. A* **356**, 3–4 (1996).
18. Andreyev, A. N. *et al.* α-decay characteristics of neutron-deficient ^{190,192}Po nuclei and alpha branching ratios of ^{186,188}Pb. *J. Phys. G* **25,** 835–837 (1999).
19. Le Coz, Y. *et al.* Evidence of multiple shape coexistence in ^{186}Pb. *Eur. Phys. J. Direct A* **3**, 1–6 (1999).
20. Cocks, J. F. C. *et al.* First observation of excited states in ^{184}Pb: spectroscopy beyond the neutron mid-shell. *Eur. Phys. J. A* **3,** 17–20 (1998).
21. Heese, J. *et al.* Evidence for low-lying prolate bands in ^{188}Pb and ^{186}Pb. *Phys. Lett. B* **302**, 390–395 (1993).
22. Baxter, A. M. *et al.* Spectroscopy of ^{186}Pb with mass identification. *Phys. Rev. C* **48,** R2140–R2143 (1993).

23. Batchelder, J. *et al.* α-decay properties of ^{190}Po and identification of ^{191}Po. *Phys. Rev. C* **55,** R2142–R2145 (1997).
24. Andreyev, A. *et al.* Fine structure in the α decay of the neutron-deficient ^{191}Po and ^{191}Bi isotopes. *Acta Phys. Pol.* **30,** 1255–1262 (1999).
25. Andreyev, A. *et al.* Hindered (Δl = 0) alpha decay and shape staggering in ^{191}Po. *Phys. Rev. Lett.* **82,** 1819–1822 (1999).
26. Wauters, J. *et al.* Fine structure in the alpha decay of even-even nuclei as an experimental proof for the stability of the Z = 82 magic shell at the very neutron-deficient side. *Phys. Rev. Lett.* **72,** 1329–1332 (1994).
27. Bijnens, N. *et al.* Intruder states and the onset of deformation in the neutron-deficient even-even polonium isotopes. *Phys. Rev. Lett.* **75,** 4571–4574 (1995).
28. Wauters, J. *et al.* Alpha decay of ^{186}Pb and ^{184}Hg: the influence of mixing of 0^+ states on α-decay transition probabilities. *Phys. Rev. C* **50,** 2768–2773 (1994).

Acknowledgements

A.N.A. is on leave from FLNPh, JINR, Dubna, Russia. We are indebted to the UNILAC staff for the excellent performance of the ion source and the accelerator. We thank the colleagues from the GSI target laboratory for the preparation of the large area $^{142}NdF_3$ targets. This work was supported by the Access to Large Scale Facility programme under the Training and Mobility of Researchers programme of the European Union, by the FWO–Vlaanderen and the GOA programme, by UK EPSRC, by the Academy of Finland and by the Swedish Natural Research Council (NFR).

Correspondence and requests for materials should be addressed to M.H. (e-mail: mark.huyse@fys.kuleuven.ac.be).

Microdomain patterns from directional eutectic solidification and epitaxy

Claudio De Rosa*†, Cheolmin Park‡†, Edwin L. Thomas‡ & Bernard Lotz§

* *Dipartimento di Chimica, Universita' di Napoli, "Federico II" Via Mezzocannone 4, 80134 Napoli, Italy*
‡ *Department of Materials Science and Engineering, Massachusetts Institute of Technology, Cambridge, Massachusetts 02139, USA*
§ *Centre de Recherches sur les Macromolecules, CNRS Strasbourg, 67083 France*
† *These authors contributed equally to this work*

Creating a regular surface pattern on the nanometre scale is important for many technological applications, such as the periodic arrays constructed by optical microlithography that are used as separation media in electrophoresis[1], and island structures used for high-density magnetic recording devices[2]. Block copolymer patterns can also be used for lithography on length scales below 30 nanometres (refs 3–5). But for such polymers to prove useful for thin-film technologies, chemically patterned surfaces need to be made substantially defect-free over large areas, and with tailored domain orientation and periodicity. So far, control over domain orientation has been achieved by several routes[6–9], using electric fields, temperature gradients, patterned substrates and neutral confining surfaces. Here we describe an extremely fast process that leads the formation of two-dimensional periodic thin films having large area and uniform thickness, and which possess vertically aligned cylindrical domains each containing precisely one crystalline lamella. The process involves rapid solidification of a semicrystalline block copolymer from a crystallizable solvent between glass substrates using directional solidification and epitaxy. The film is both chemically and structurally periodic, thereby providing new opportunities for more selective and versatile nanopatterned surfaces.

Block copolymers consist of chemically distinct macromolecules covalently linked to form a single chain; due to their mutual repulsion, the dissimilar blocks tend to segregate into different domains whose shape, size and spacing are determined by the relative amount of the block components and their respective molecular masses[10,11].Control over the microdomain patterns has been achieved by employing electric fields, temperature gradients, patterned substrates and neutral confining surfaces. For example, a temperature gradient has been used[12] to produce a vertically aligned lamellar structure with excellent long-range order. To obtain a well ordered structure, slow growth (millimetres per day) in a large gradient (700 °C per centimetre) is required.

In crystalline materials, control of the solidification process is central to many technologies that rely on the features of the resultant microstructure for achieving optimum properties. For example, the directional solidification of a eutectic metal alloy can lead to rod or lamellar structures well aligned along the growth direction[13]. In crystalline polymeric materials, orientation of crystallizable macromolecules has been achieved by mechanical forces, as in fibre spinning and also by epitaxial crystallization onto substrates[14,15]. A vertically oriented lamellar structure has been achieved[16] by utilizing crystallization from the microphase-separated state of a low-molecular-mass diblock copolymer adjacent to boundaries formed by dewetting from the substrate. Mixtures of polyethylene and a crystallizable solvent (tetrachlorobenzene) form a binary eutectic[17], and polyethylene homopolymer has been shown[18] to epitaxially crystallize on benzoic acid. We also note that benzoic acid and paraffin have been shown[19] to form a eutectic, and that the paraffin grows epitaxially onto the crystallized benzoic acid. We thus considered that a semicrystalline block copolymer dissolved in a crystallizable and epitaxy-forming solvent might yield interesting directionally solidified structures.

We used a polystyrene-block-polyethylene (PS-PE) diblock copolymer that was prepared by hydrogenation of polystyrene-block-1,4-butadiene, previously synthesized via sequential anionic polymerization. The amorphous PS block and the crystallizable PE block have molecular masses of 40,000 and 10,000 daltons respectively, the volume fraction of the PE block is 0.24, and the melting point of the PE block is 98 °C. Small-angle X-ray scattering measurements of bulk films of PS-PE shows multiple low-angle reflections characteristic of hexagonally packed PE cylinders with the first Bragg peak at $q = 0.15\ nm^{-1}$, corresponding to a cylinder–cylinder spacing of 42 nm. (Here $q = (4\pi/\lambda)\sin\theta$, where λ is the X-ray wavelength and θ is 1/2 of the scattering angle.)

When cast from dilute xylene solution onto a carbon support film, the structure consists of in-plane meandering cylinders of PE in the PS matrix (Fig. 1a). In order to control the PS-PE microdomain and crystalline PE structures, we first dissolved the diblock in benzoic acid (BA), then crystallized the solution between glass slides in two stages using a modest temperature gradient ($10\ °C\ cm^{-1}$). In the first directional solidification done at 110 °C, the BA forms large 200 × 500 μm crystals with the (001) planar surfaces parallel to the substrate and the *b* axis (the fast growth direction) well aligned along the temperature gradient. The remaining solution is then directionally solidified at 60 °C. A thin polymer layer forms adjacent to the glass surfaces, and can be examined by microscopy. A bright field image of the RuO_4-stained film shows well ordered arrays of light, unstained PE domains in a dark, stained PS matrix (Fig. 1b). The light domains are packed on a hexagonal lattice with good long-range order extending over areas of 20 μm diameter.

Tilting the film in the transmission electron microscope (TEM) shows that the light domains are cylindrical rather than spherical. A magnified image shows that the shape of the interface between the PS and PE is non-circular (Fig. 1b inset). The diameter of the PE domains along the b_{BA} direction is about 50% larger on average than in the perpendicular direction (30 nm compared to 20 nm). We will come back to this point later in the context of the dark-field images and the mechanism of structure formation.

An electron diffraction pattern from an unstained film (Fig. 2A) shows very well oriented, almost single-crystal-like, reflections